Am J Transl Res 2016;8(6):2693-2704
www.ajtr.org /ISSN:1943-8141/AJTR0027308

Original Article

Reconstructing jaw defects with MSCs and PLGA-encapsulated growth factors

Boon Ching Tee[1], Kashappa Goud H Desai[2,6], Kelly S Kennedy[3], Brittany Sonnichsen[3], Do-Gyoon Kim[4], Henry W Fields[4], Susan R Mallery[5], Steven P Schwendeman[2], Zongyang Sun[4]

[1]Division of Biosciences, College of Dentistry, The Ohio State University, Columbus, Ohio, USA; [2]Departments of Pharmaceutical Sciences and Biomedical Engineering, The Biointerfaces Institute, University of Michigan, Ann Arbor, Michigan, USA; [3]Division of Oral and Maxillofacial Surgery, College of Dentistry, The Ohio State University, Columbus, Ohio, USA; [4]Division of Orthodontics, College of Dentistry, The Ohio State University, Columbus, Ohio, USA; [5]Division of Oral Pathology & Radiology, College of Dentistry, The Ohio State University, Columbus, Ohio, USA; [6]Current Address: GlaxoSmithKline, King of Prussia, PA 19406, USA

Received March 4, 2016; Accepted May 7, 2016; Epub June 15, 2016; Published June 30, 2016

Abstract: Cell and growth factor-based tissue engineering has shown great potentials for skeletal regeneration. This study tested its feasibility in reconstructing large mandibular defects and compared the efficacy of varied construction materials and sealing methods. Bilateral mandibular critical-size (5-cm^3) defects were created on six 4-month-old domestic pigs, and grafted with β-tricalcium phosphate (βTCP) only (Group-A), βTCP with autologous bone marrow-derived mesenchymal stem cells (BM-MSCs) (Group-B), and βTCP with BM-MSCs and biodegradable poly(lactic-co-glycolic acid) (PLGA) microspheres containing bone morphogenetic protein-2 (BMP-2) and vascular endothelial growth factor (VEGF) (Group-C). The buccal sides of Groups-B/-C were either sealed by fibrin sealant or by a biodegradable PLGA barrier membrane before soft-tissue closure. Computed tomography (CT), microCT and histology analyses were performed 12 weeks postoperatively. *In vitro* data demonstrated that BM-MSCs, with MSC properties confirmed, remained vital after integration with βTCP; and PLGA microspheres exhibited an initial burst followed by slow and continuous release of growth factors over a period of 28 days. *In vivo* data demonstrated that Group-B/-C sites had significantly greater gap obliteration, higher tissue mineral densities and more residual βTCP granules ($p<0.05$, Kruskal-Wallis tests). Qualitatively, Group-B/-C defect sites had started remodeling while Group-A sites were mainly forming new bone to bridge the gaps. Furthermore, βTCP degradation was not mediated by macrophages or osteoclasts, and was significantly slowed down by sealing the defects with barrier membrane. Combined, these data present a promising formulation composed of βTCP granules, autologous MSCs, controlled-release growth factors and biodegradable PLGA barrier membrane for the reconstruction of critical-size mandibular defects.

Keywords: Bone tissue engineering, critical-size mandibular defect, bone marrow-derived mesenchymal stem cells, controlled-release growth factors, biodegradable barrier membrane

Introduction

For decades, reconstruction of large mandibular skeletal defects has relied on autologous, allogeneic or synthetic bone grafts, which have major disadvantages including donor site morbidity, transplant rejection, and lack of osteoconductivity, respectively [1, 2]. Recent advances in tissue engineering have confirmed the plausibility of treating large defects through a "graft-free" approach [3-5]. By mimicking the biological process of natural bone healing, biomaterial scaffolds, self-renewal cells, and bioactive molecular factors can be assembled together to replace bone grafts. Likewise, recent clinical case reports have confirmed the efficacy of using mesenchymal stem cells (MSCs) and osteoconductive scaffolds for reconstructing maxillary defects [6, 7], although its efficacy for mandibular defects was found to be unpredictable [8].

β-Tricalcium phosphate (βTCP) has been found by several clinical and animal studies to be a promising scaffold material for mandibular defects [9, 10]. However, it does have a disad-

vantage of being degraded faster than new bone regeneration occurs [11]. In addition, implanting βTCP alone only has a moderate regenerative efficacy [12, 13]. After being integrated with MSCs, the regenerative efficacy can be substantially enhanced as shown from calvarial [5], femoral [14] and alveolar [15] defect studies. During normal bone healing, MSCs are recruited to the defect site to replace damaged cells by differentiating into functional cells [16], secrete immunoregulatory factors to mediate inflammation [17], and produce growth factors to initiate angiogenesis and osteogenesis [17, 18]. Being integrated with βTCP, exogenous MSCs can be brought to the defect site to carry out the bone healing mechanism. To date, however, few studies have tested bone regeneration effects of βTCP combined with MSCs for mandibular defect reconstruction, and the outcomes have been inconsistent [19].

Besides MSCs, growth factors are also important for initiating and maintaining defect regeneration. Among a variety of growth factors, bone morphogenetic proteins (BMP) and vascular endothelial growth factor (VEGF) have been confirmed to be critical for osteogenesis and vascularization, respectively [3, 20]. They also stimulate cell proliferation, migration, and differentiation. While they may be secreted by native and recruited osteogenic or angiogenic cells at the defect sites, the process is slow and the amount is inadequate. In small animal model studies, dual delivery of exogenous BMP-2 and VEGF has been found to synergistically improve bone regeneration [3, 20-23]. However, little is known about their interaction with transplanted MSC. Furthermore, both growth factors are known to have short half-lives, and injection or collagen sponge delivery of them require high concentrations and multiple doses, increasing the risk to complications such as vascular malformation and heterotopic ossification [24]. To sustain activity and minimize complications, controlled release of these factors is desired. Previous work has confirmed that injectable poly(lactic-co-glycolic acid) (PLGA) microparticles represent an important platform for controlled-release applications [25]. However, owing to protein instability during encapsulation and release, achieving effective PLGA microencapsulation and slow and continuous release of BMP2 and VEGF for mandibular defects can be challenging [25, 26].

Therefore, the purpose of this study was to test the efficacy of a new formulation consisting βTCP, BM-MSCs, PLGA-encapsulated slow-release BMP2 and VEGF together with barrier membranes, in reconstructing critical-size mandibular defects in a preclinical pig model. We hypothesized that adding MSCs would have a significantly stronger regenerative efficacy than βTCP alone, while adding PLGA-microencapsulated controlled-release BMP2 and VEGF would have even stronger efficacy than MSCs and βTCP, and the use of barrier membranes would slow down βTCP degradation and enhance bone regeneration.

Materials and methods

Materials

PLGA 50:50 was purchased from Boehringer-Ingelheim GmbH (Ingelheim, Germany). VEGF and BMP-2 were donated by Genentech Inc. (South San Francisco, CA, USA) and Pfizer (Cambridge, MA), respectively. Cerasorb® M βTCP granules and Inion PLGA membrane were purchased from Curasan, Inc (Durham, NC), while Tisseel fibrin sealant from Baxter International Inc. (Deerfield, IL). All cell culture reagents were purchased from Life Technologies (Carlsbad, CA) unless otherwise stated.

Animals

Six 4-month-old female domestic pigs (*Sus scrofa*), 30-35 kg in weight, divided into 3 groups (A, βTCP only; B, βTCP + BM-MSCs; C, βTCP + BM-MSCs + growth factors; 4 defect sites/group) were used for *in vivo* experiments. All live animal procedures were approved by The Ohio State University Institutional Animal Care and Use Committee.

BM-MSC isolation, expansion, and integration into βTCP granules

Bone marrow was aspirated from the pig tibia, from which BM-MSCs were isolated, characterized and expanded following procedures detailed previously [27]. Autologous BM-MSCs within passage 3-5 were integrated with βTCP granules and used for *in vivo* transplantation (for Groups-B/-C). Briefly, 1 day before transplantation, 10 mL βTCP granules (diameter 1000-2000 μm) were divided into two conical tubes and coated with CTS CELLstart substrate

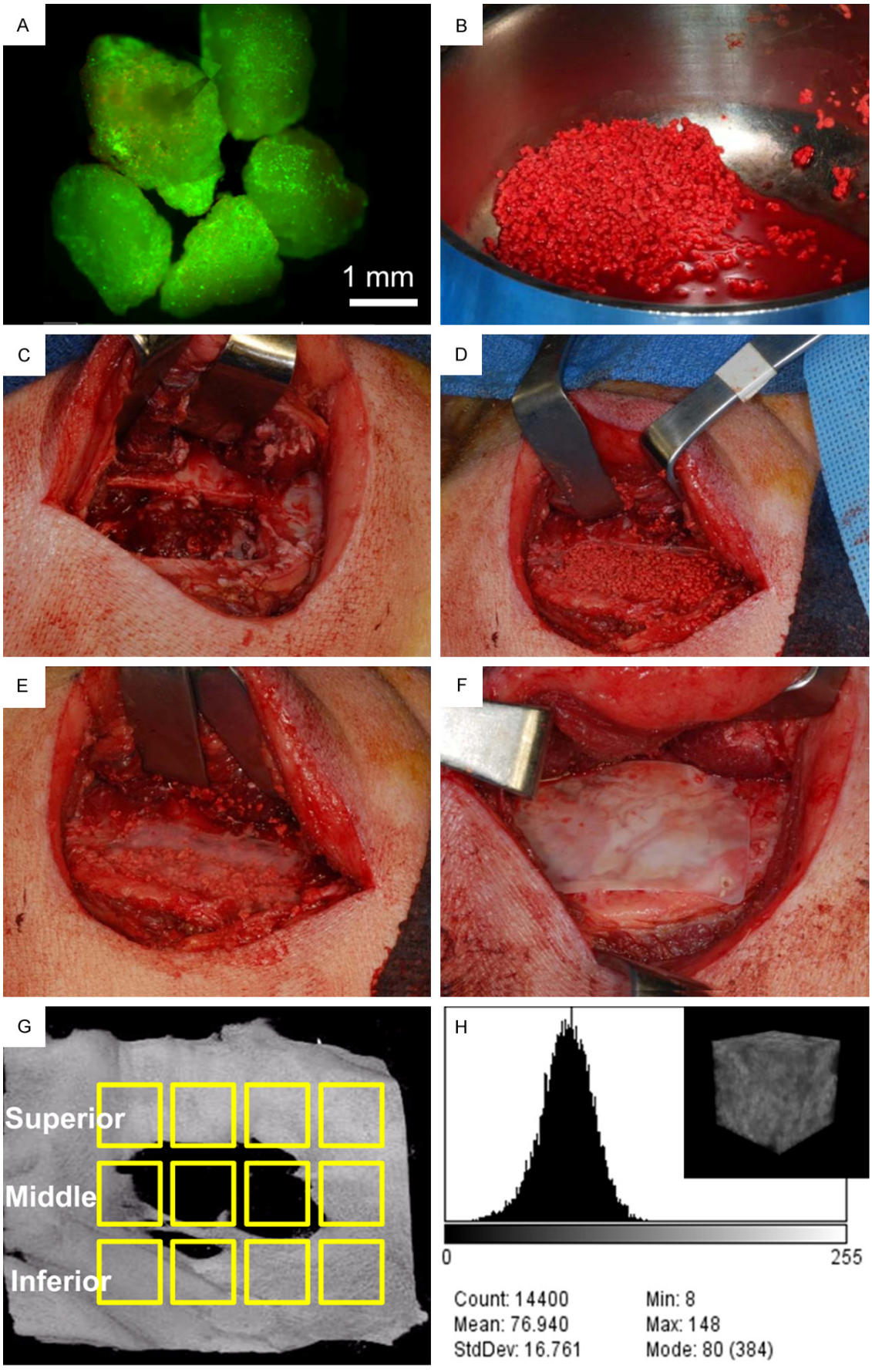
A
1 mm
B
C
D
E
F
G
Superior
Middle
Inferior
H
0
255
Count: 14400
Mean: 76.940
StdDev: 16.761
Min: 8
Max: 148
Mode: 80 (384)

Figure 1. Illustrations of methods. A. MSC-integrated βTCP were stained with calcein AM (green; live cells) and ethidium homodimer-1 (red; dead cells). B. Graft materials were mixed with autologous blood in a sterile bowl during the surgery. C. An osteotomy of 5.0 cm^3 was performed at the lateral aspect of the mandible. D. Graft materials were impacted to the defect site. E. Graft materials were covered by fibrin sealant. F. A barrier membrane was screwed onto the buccal surface to seal the graft materials. G. The reconstructed images of a defect site from microCT scan were separated into 3 levels-superior, middle, inferior-and 4 identical cubes were isolated from each level. H. The histogram of the cubes isolated from microCT images was generated by ImageJ software.

at 37°C for 3 hrs. Then, BM-MSCs were trypsinized, resuspended in StemPro MSC serum-free media (SFM) and centrifuged twice with βTCP at 400 rpm for 5 min. MSC-integrated βTCP were then spread out on a 60-mm ultra-low attachment culture dish (Corning, Corning, NY) and cultured in StemPro SFM overnight. Several granules were removed to assess cell viability using a Live/Dead Viability/Cytotoxicity kit for mammalian cells (**Figure 1A**). An average of 3.5 ± 1.6×10^7 BM-MSCs were integrated into 5 ml of βTCP granules for each defect site.

Preparation of VEGF or BMP-2 encapsulated PLGA microspheres

Several formulation and preparation variables were evaluated to determine optimal conditions for effective encapsulation of growth factors in PLGA microspheres (Supplementary Tables 1-3; Supplementary Figure 1). The procedure (water-in-oil-in-water (w/o/w) emulsion solvent evaporation) adopted to prepare the optimal BMP2 and VEGF microsphere formulations for *in vivo* experiments is as follows (**Table 1**). An inner water phase was added to an oil phase and homogenized in an ice/water bath to obtain primary w/o emulsion. About 2 mL of 5% polyvinyl acetate (PVA) solution was added to the above formed emulsion and vortexed for 1 min to form w/o/w emulsion. The resultant emulsion was poured into 100 mL of 0.5% PVA solution under magnetic stirring and hardened at room temperature for 3 h. Hardened microspheres were collected by sieve (20-63 μm), washed repeatedly with double-distilled H_2O, and freeze-dried. Surface morphology of microspheres was examined by scanning electron microscopy (SEM) (Supplementary Data).

Evaluation of in vitro release of active VEGF and BMP-2 from PLGA microspheres

About 7 mg of VEGF encapsulated or 5 mg BMP-2 encapsulated microspheres were incubated in appropriate release medium at 37°C under constant agitation (240 rpm/min). At different incubation times (1, 3, 7, 14, 21 and 28 days), the supernatant was collected and analysis of released active VEGF or BMP-2 was performed by ELISA (Supplementary Data).

Surgery for critical-size defect creation, impaction and postoperative procedures

Bilateral critical-size mandibular osteotomies of 5.0 cm^3 (width/height/depth, 3.5×1.5×1 cm) were created on anesthetized pigs following previously established procedures [28] (**Figure 1C**).

After thoroughly cleansing bone debris, the defect was filled with βTCP only (Group-A; n=4), βTCP integrated with MSCs (Group-B; n=4) and βTCP integrated with MSCs and growth factors (Group-C; n=4) (**Figure 1D**), coagulated with autologous pig blood at the surgical table (**Figure 1B**). On the buccal side, as the periosteum was removed, the grafted materials were sealed either by 1.5-mL fibrin sealant (4 control sites, 4 experimental sites) or by 1.5-mL fibrin sealant with barrier membrane (4 experimental sites). The surgical field was cleaned, repositioned and closed by suturing the overlying soft tissues.

Postoperative pain and infection control was provided as detailed previously [28]. Fluorescent dyes calcein and alizarin-3-methyliminodiacetic acid (Sigma-Aldrich) were administered intravenously during postoperative week-10 and -11, respectively, following methods previously reported [28], and euthanized at week-12.

Multislice computed tomography (CT) scans and geometric analysis of defect regeneration

Each pig head was scanned using a GE LightSpeed 8-multidetector helical CT scanner (Buckinghamshire, UK) at 0.625-mm slice thickness and the geometric analysis was performed as previously reported [28]. The horizontal and vertical widths of the remaining defect were measured using MIMICS 10.01 (Materialise, Plymouth, MI).

Table 1. The formulation conditions for PLGA microspheres encapsulated with VEGF and BMP2, and evaluation of encapsulation efficiency

Formulation conditions and compositions	VEGF formulations	BMP-2 formulations
PLGA concentration (mg/mL)	500	500
Inner water phase volume (mL/1 mL oil phase)	0.2	0.2
First homogenization speed (rpm)	10,000	10,000
First homogenization duration (min)	1	1
Second vortexing time (min)	1	1
VEGF or BMP-2 loading (wt%)	0.1	0.2
BSA loading (wt%)	2.7	0.3
$MgCO_3$ loading (wt%)	3.0	3.0
Evaluation of microencapsulation		
Theoretical loading (wt%)	0.1	0.2
Actual loading (wt%)	0.03 ± 0.005	0.06 ± 0.002
Actual loading (wt%)-total protein	2.2 ± 0.12	0.4 ± 0.01
Encapsulation efficiency (%)	37.1 ± 5.0	37.7 ± 1.0
Encapsulation efficiency (%)-total protein	78.8 ± 4.1	72.2 ± 3.1

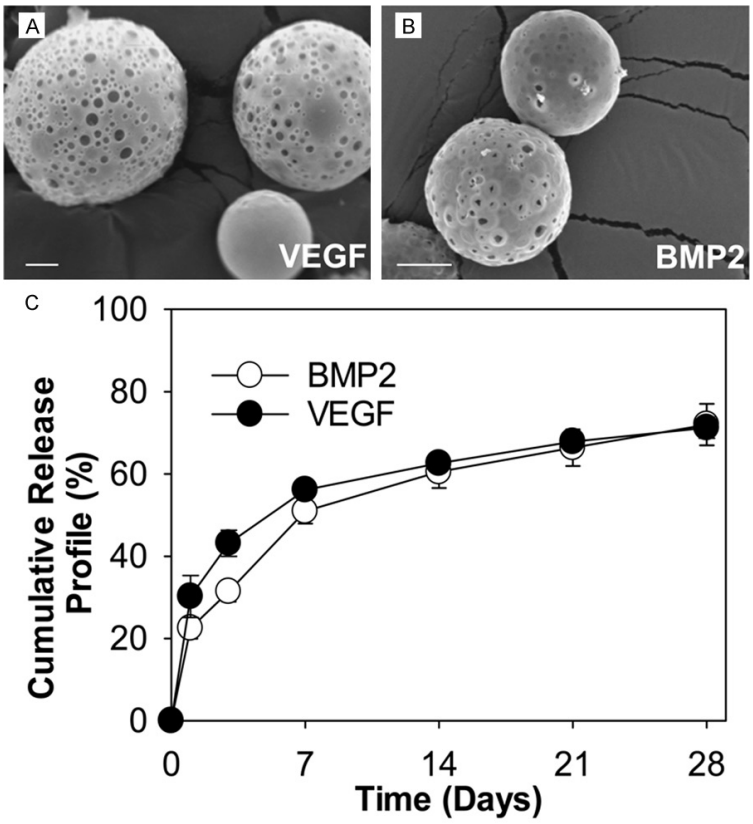

Figure 2. PLGA microsphere preparation and results. (A, B) Surface morphology (SEM images) of the PLGA microspheres loaded with VEGF (A) and BMP2 (B). (C) *In vitro* release (cumulative amount of active VEGF or BMP2 released as a function of incubation time) characteristics of PLGA microspheres loaded with VEGF and BMP2. *In vitro* release was conducted in PBS + 0.02% Tween 80 + 1% BSA (VEGF release medium) or PBS + 0.02% Tween 80 + 1% BSA + 0.15 % w/v EDTA (BMP2 release medium) at 37°C. Symbols represent mean ± SEM (n = 3). Scale bars = 20 μm.

MicroCT scans and analysis of tissue mineral density at the defect area

By referring to the tantalum beads shown on multislice CT scan, specimens containing the original defect and 0.5-1.0 cm of old bone were collected and underwent microCT scans with SkyScan 1172 (Kontich, Belgium) at 27-μm voxel size [28]. Using ImageJ (NIH, Bethesda, MD), four 34 mm^3 cubes were isolated from the superior, middle, and inferior parts of the defect area (**Figure 1G**). Tissue mineral density (represented by mean gray value) of each cube was obtained by dividing the sum of gray values by the total count of bone voxels in the cube (**Figure 1H**).

Histology

After microCT scan, each specimen was divided into superior and inferior pieces and processed for undecalcified and decalcified histology, respectively, following protocols established previously [28]. Undecalcified sections were used to assess mineral apposition and healing characteristics. Decalcified sections, stained by hematoxylin and eosin (H&E), were used to assess general histology and quantify residual βTCP granules.

Statistical analysis

Normality of data distribution was assessed using Shapiro-Wilk tests. Defect geometric measurements, tissue mineral density, and the relative amount of residual βTCP from 3 independent samples were compared by non-parametric Kruskal-Wallis tests. An α=0.05 was adopted.

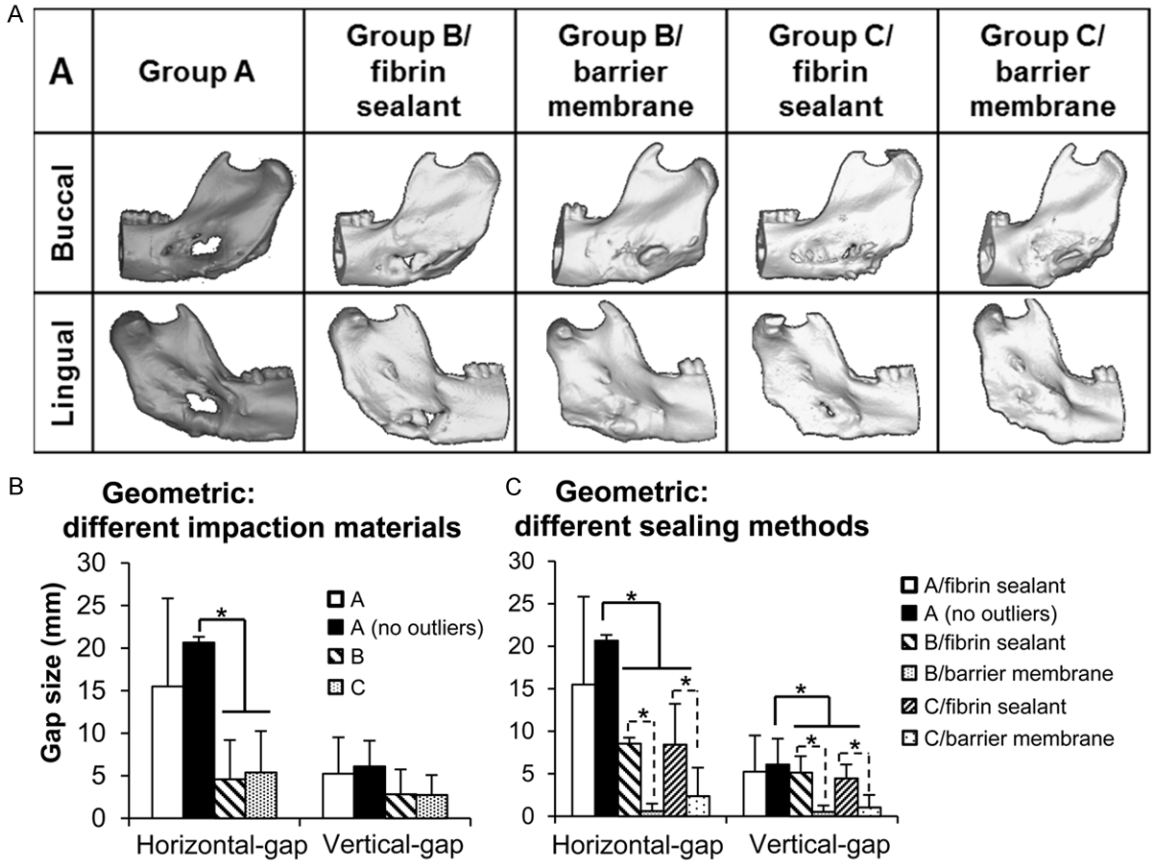

Figure 3. Geometric analyses for the effects of MSC and MSC/growth factors on bone regeneration. A. Volumetric surface reconstruction of representative samples from CT images. All control defects (Group-A) had large through-and-through defect except for an outlier. All experimental defects (Groups-B and -C) had significant gap obliteration, but complete union only occurred in defects sealed with barrier membranes. B. The addition of MSCs (Group-B) and MSC/growth factors (Group-C) significantly reduced the horizontal-gap width when compared to Group-A without the outlier. C. The use of barrier membrane significantly reduced both horizontal and vertical widths regardless of the graft materials. Bars represent mean ± SD; *P < 0.05, Kruskal-Wallis tests.

Results

Evaluation of PLGA microencapsulation and in vitro release of VEGF and BMP2

The PLGA microsphere formulation with optimal loading capacity and efficiency, and *in vitro* release behavior (slow and continuous release of active growth factors) was chosen for *in vivo* evaluation (**Table 1**, **Figure 2**).

Multislice CT and geometric analyses of bone regeneration

In Group-A (control), all defect sites except one outlier had large through-and-through defects present (**Figure 3A**). In contrast, all sites in the experimental groups (Group-B and -C) only showed small through-and-through defects, with the horizontal-gap size significantly smaller than Group-A without the outlier (**Figure 3A**).

For the experimental groups, the size of the remaining site was not changed significantly by growth factors (**Figure 3B**), but by the sealing methods (**Figure 3C**). Regardless of the impaction materials, the 4 experimental defects sealed by fibrin sealant and barrier membrane showed negligible gaps (< 1.50 mm), significantly smaller than the 4 experimental defects sealed by fibrin sealant only (**Figure 3C**).

MicroCT and tissue mineral analyses of bone regeneration

The mean tissue mineral density was higher in Groups-B and -C than in Group-A (**Figure 4B**), although only the middle portion reached sig-

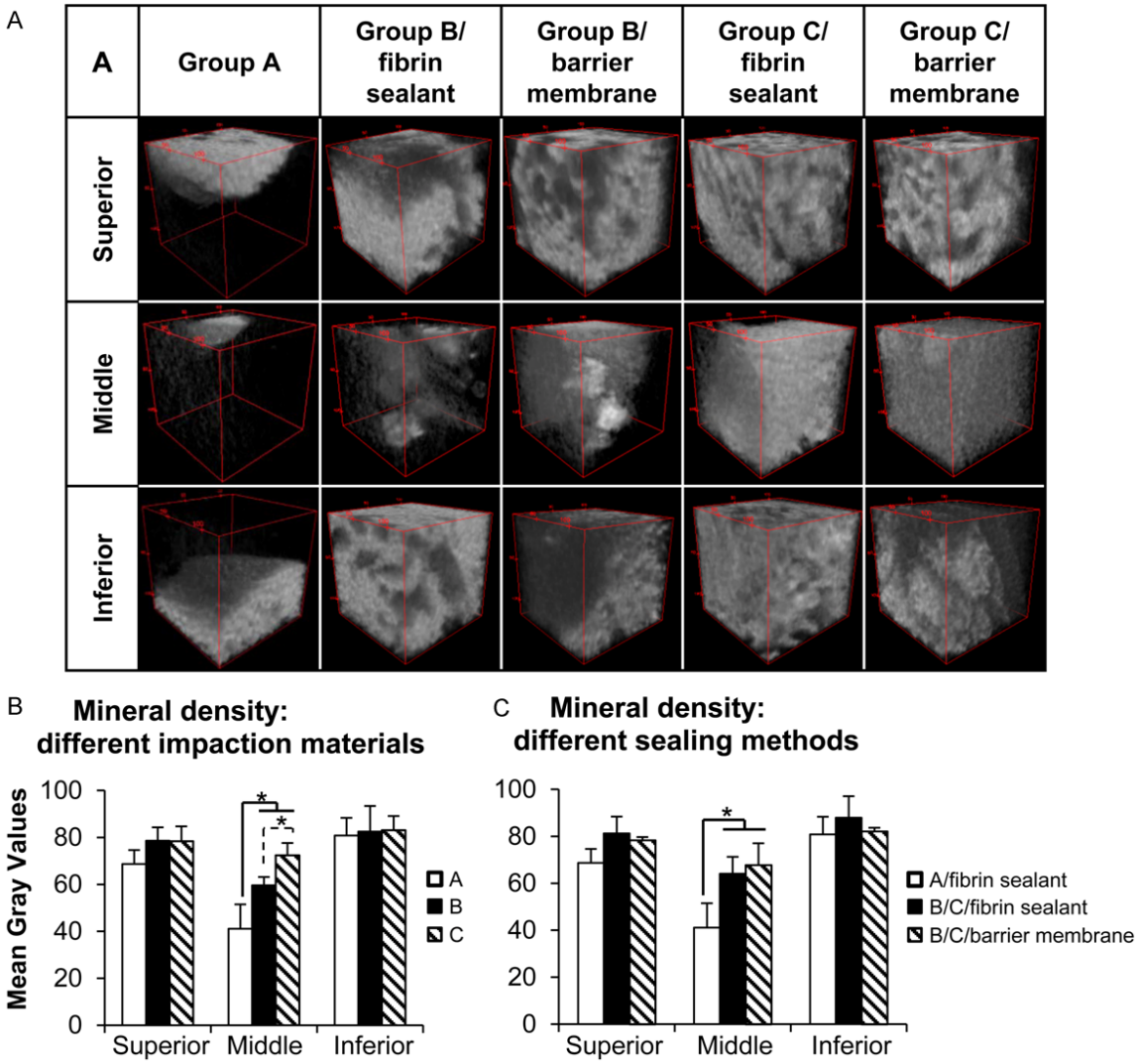

Figure 4. Tissue mineral density analyses for the effects of MSC and MSC/growth factors on bone regeneration. A. Volumetric reconstruction of the representative samples from the cubes isolated from microCT images. B. Both impaction materials significantly improved tissue mineral density in the middle portion of the defect, and the addition of MSC/growth factors (Group-C) was superior to the addition of MSCs only (Group-B). C. The sealing methods did not make a difference to the tissue mineral density. Bars represent mean ± SD; *P < 0.05, Kruskal-Wallis tests.

nificance. Comparison between Groups-B and -C showed that adding growth factors further increased tissue mineral density significantly (**Figure 4B**). Tissue mineral density was not different between the two sealing methods (**Figure 4C**).

Analysis of undecalcified histology

Most defect sites in Group-A showed active bone growth, represented by green and red fluorescent labels, at the bone fronts towards the defects (**Figure 5A**); whereas Groups-B/-C mostly showed bridging of the defects and bone remodeling, represented by resorptive cavities and secondary osteons (**Figure 5B** and **5C**). In sites sealed by both fibrin sealant and barrier membrane, new bones grew over the membrane (**Figure 5C**).

Analysis of decalcified histology

Group-A showed new woven bones extended and tapered towards the remaining defects which were filled by fibrous tissues and blood vessels, while Groups-B and -C defects were largely obliterated. Osteoclasts were present at the barrier membrane, bone marrow and corti-

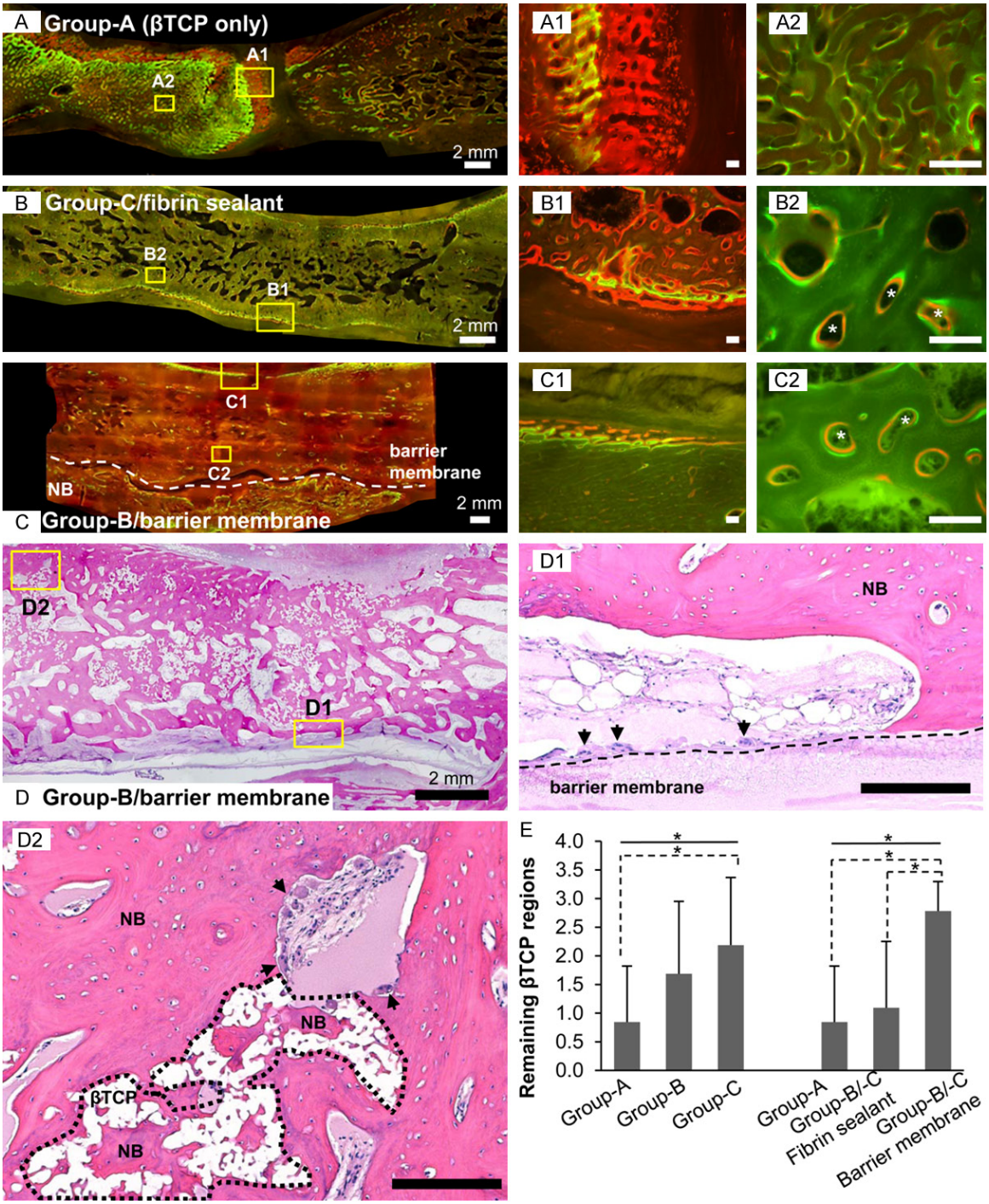

Figure 5. Histology analyses to assess mineral apposition and residual βTCP at the defect sites. A. In control Group-A, active bone growth was present at the bone fronts toward the defects. B. With the addition of MSC (Group-B; not shown) and MSC/growth factor (Group-C), the defects were completely fused, active mineral apposition was only present along the buccal and lingual surfaces (B1) and remodeling of new bone (represented by secondary osteons, *) had started. C. When sealed by a barrier membrane, both experimental Group-B and Group-C (not shown) had completely reconstructed defects with extensive new bone growth over the barrier membrane. (A1, B1, C1) High magnification images showing active mineral deposition at the gap (A1), buccal (B1), and lingual (C1) surfaces. (A2, B2, C2) High magnification images showing active bone remodeling in the newly-regenerated bone regions. D. HE image showing residual βTCPs in the defect site. (D1) High magnification image showing the presence of osteoclasts underneath the barrier membrane (arrows). (D2) High magnification image showing the absence of osteoclasts around residual βTCP, but present at some buccal and lingual bone surfaces as well as the bone marrow surfaces.

E. The addition of both MSC (Group-B) and MSC/growth factors (Group-C) increased the amount of residual βTCP, but the change was only significant with MSC/growth factors (Group-C). When the defects were sealed with barrier membrane, the amount of residual βTCP was significantly higher than those sealed with fibrin sealant. Bars represent mean ± SD; *P < 0.05, Kruskal-Wallis tests. Scale bars = 200 μm unless otherwise stated.

cal surfaces, but not around residual βTCPs (**Figure 5D**). The amount of residual βTCP was significantly greater in Groups-B/C than in Group-A, as well as in sites sealed by both fibrin sealant and barrier membrane than by fibrin sealant alone (**Figure 5E**).

Discussion

Using a pig critical-size mandibular defect model, this study directly compared the osteogenic regenerative efficacy of βTCP with and without the addition of autologous BM-MSCs and growth factors. Overall, the data confirmed our initial hypothesis that MSCs would significantly augment the regenerative efficacy of βTCP. Adding PLGA-microencapsulated controlled-release BMP2 and VEGF tended to further enhance the regenerative efficacy of βTCP and BM-MSCs, but the difference was less than we initially hypothesized.

The positive bone regenerative capacity of BM-MSCs for mandibular defects found in this study is consistent with those found from calvarial [5], femoral [14] and alveolar [15] sites. Specifically, BM-MSCs significantly improved both new bone quantity represented by geometric changes (**Figure 4A** and **4B**) and new bone quality represented by tissue mineral density (**Figure 4C** and **4D**) at the defect sites. These findings confirm that despite the differences in anatomy and function in cranial bone and long bone, the mandible is amenable to the therapy of combined βTCP and BM-MSC treatment. Analysis of dynamic mineral apposition further found that sites treated by BM-MSCs have mostly bridged the defects and started remodeling (**Figure 5B-D**), while sites treated by βTCP alone were still forming woven bones for purpose of bridging the defect (**Figure 5A**). This difference confirms that when only βTCP was used, recruitment of endogenous MSCs there is slow and inadequate [29], which can be augmented by exogenous MSCs transplantation.

In regard to the finding that the addition of PLGA-encapsulated BMP2 and VEGF in transplanted MSC only had limited efficacy in further stimulating osteogenesis at the mandibular defect sites, there may be two explanations. First, it is possible that BM-MSC alone has secreted adequate endogenous growth factors which stimulated the regeneration to a fairly optimal level [17, 18], leaving little room for further improvement by the exogenous growth factors. This interpretation is well substantiated by the fact that most of the defect sites receiving MSCs with and without growth factors already had fully bridged defects (**Figure 3**), and mineral activity has shifted from fast bone formation to bone remodeling (**Figure 5**). Second, the effectiveness of dual delivering BMP2 and VEGF may be suboptimal. Although several studies found that simultaneous delivery of BMP2 and VEGF enhances bone regeneration [3, 20], others have suggested that dual delivery is inefficient in orthotopic bone healing [30] and bone regeneration effects of BMP2 may even be inhibited by VEGF [31, 32]. Some researchers further proposed that VEGF and BMP2 should be administered sequentially for optimal effects [22, 33]. While our findings seem to be consistent with this notion, whether and how VEGF and BMP2 should be sequentially administered for mandibular defect reconstruction need to be further investigated.

Nevertheless, our extensive *in vitro* work on PLGA microencapsulation for long-term release of BMP2 or VEGF has made the sequential *in vivo* delivery of these BMP2 and VEGF feasible. Owing to undesirable stresses such as aqueous/organic interface, heat and shear during microencapsulation, the encapsulated growth factors may have substantial protein denaturation and variability in protein release [34, 35]. To minimize protein denaturation during primary emulsification, stabilizing excipients (e.g., bovine serum albumin, poloxamer 407, cyclodextrin, trehalose) have been co-incorporated in an inner water phase [36]. In this study, we incorporated bovine serum albumin to minimize the instability of VEGF and BMP2 during PLGA microencapsulation, and optimized other important variables (e.g., inner water phase volume and concentration and M_w of PLGA) [25]. Our data demonstrate that the w/o/w emulsion-solvent evaporation method provided

more effective encapsulation and better controlled-release of active growth factors than s/o/w emulsion-solvent evaporation (Supplementary Table 2; Supplementary Figure 1). The optimal primary emulsification conditions (**Table 1**) yielded PLGA microspheres that exhibited better encapsulation efficiency as well as slow and continuous release of active growth factors. In addition, with co-encapsulation of basic salt such as $MgCO_3$ to neutralize the acidic microclimate produced by PLGA degradation [34, 35], slow and continuous release of active proteins and peptides over an extended period of time (1 month) are achieved (**Figure 2C**).

Another main finding pertains to the degradation of the scaffold materials, βTCP. Ideally, the rate of scaffold degradation should match the rate of tissue regeneration. In this study, we found that the *in vivo* degradation rate of βTCP granules decreased when integrated with autologous BM-MSCs and growth factors, or when they were contained by the barrier membrane. Two factors may account for these changes. First, VEGF and BMP2 may have induced local MSC proliferation, collagen network formation and mineral apposition, thereby enhancing the weight-loading capacity of βTCP and delayed its dissolution and degradation. Consistent with this explanation, similarly delayed degradation has been found in an *in vitro* model using collagen/βTCP composite scaffold [37]. Next, as our data demonstrated that no osteoclasts were associated with βTCP degradation, indicating βTCP degradation is very likely through hydrolysis mediated by tissue fluid instead of ingestion or resorption mediated by cells. This point is shared by some [38, 39] but not by others [4, 40]. Nevertheless, the hydrolytic degradation mechanism provides a reasonable explanation for the faster degradation of βTCP in defect sites where no MSCs/growth factors were involved and no barrier membrane was used. More specifically, while fibrin sealant alone does not prevent tissue fluid flow in and out of the defect, when a barrier membrane is secured overlying βTCP and exposed to tissue fluid, it stiffens and encloses the graft materials and reduces tissue fluid flow at the defect site, consequently delaying the degradation of βTCP. Therefore, the addition of MSCs and growth factors and the use of a barrier membrane help match the degradation rate of βTCP and bone regeneration rate better than using βTCP alone without an overlying membrane.

Overall, as with many early stage studies, this study had a relatively small sample size, which prohibited the collection of longitudinal angiogenesis/osteogenesis data at multiple time points and a definite conclusion about the BMP/VEGF effects. Despite this limitation, this study presents three important findings: 1) using a water/oil/water emulsion-solvent method and co-encapsulation with magnesium carbonate ($MgCO_3$), BMP2 and VEGF can be encapsulated with PLGA for extended slow-release; 2) autologous BM-MSCs and slow-release growth factors can be used together with βTCP to significantly enhance reconstruction of critical-size mandibular defects; and 3) a biodegradable PLGA barrier membrane can be used to secure the constructing material and better match βTCP degradation with tissue engineering. Based on these findings, future work will further optimize the sequence, timing of growth factor delivery together with MSCs for reconstruction of critical-size mandibular defects.

Acknowledgements

This study was supported by a research support grant from Oral and Maxillofacial Surgery Foundation and a seed grant from The Ohio State University College of Dentistry.

Disclosure of conflict of interest

None.

Address correspondence to: Zongyang Sun, Division of Orthodontics, College of Dentistry, The Ohio State University, 4088 Postle Hall, 305 W 12th Ave, Columbus, OH 43210, USA. Tel: 614-247-7944; Fax: 614-688-3077; E-mail: sun.254@osu.edu

References

[1] Rogers GF and Greene AK. Autogenous bone graft: basic science and clinical implications. J Craniofac Surg 2012; 23: 323-327.

[2] Athanasiou VT, Papachristou DJ, Panagopoulos A, Saridis A, Scopa CD and Megas P. Histological comparison of autograft, allograft-DBM, xenograft, and synthetic grafts in a trabecular bone defect: an experimental study in rabbits. Med Sci Monit 2010; 16: BR24-31.

[3] Patel ZS, Young S, Tabata Y, Jansen JA, Wong ME and Mikos AG. Dual delivery of an angiogenic and an osteogenic growth factor for bone regeneration in a critical size defect model. Bone 2008; 43: 931-940.
[4] Kucera T, Sponer P, Urban K and Kohout A. Histological assessment of tissue from large human bone defects repaired with beta-tricalcium phosphate. Eur J Orthop Surg Traumatol 2014; 24: 1357-1365.
[5] Del Rosario C, Rodriguez-Evora M, Reyes R, Delgado A and Evora C. BMP-2, PDGF-BB, and bone marrow mesenchymal cells in a macroporous beta-TCP scaffold for critical-size bone defect repair in rats. Biomed Mater 2015; 10: 045008.
[6] Mesimaki K, Lindroos B, Tornwall J, Mauno J, Lindqvist C, Kontio R, Miettinen S and Suuronen R. Novel maxillary reconstruction with ectopic bone formation by GMP adipose stem cells. Int J Oral Maxillofac Surg 2009; 38: 201-209.
[7] Shayesteh YS, Khojasteh A, Soleimani M, Alikhasi M, Khoshzaban A and Ahmadbeigi N. Sinus augmentation using human mesenchymal stem cells loaded into a beta-tricalcium phosphate/hydroxyapatite scaffold. Oral Surg Oral Med Oral Pathol Oral Radiol Endod 2008; 106: 203-209.
[8] Meijer GJ, de Bruijn JD, Koole R and van Blitterswijk CA. Cell based bone tissue engineering in jaw defects. Biomaterials 2008; 29: 3053-3061.
[9] Knabe C, Koch C, Rack A and Stiller M. Effect of beta-tricalcium phosphate particles with varying porosity on osteogenesis after sinus floor augmentation in humans. Biomaterials 2008; 29: 2249-2258.
[10] Sohier J, Daculsi G, Sourice S, de Groot K and Layrolle P. Porous beta tricalcium phosphate scaffolds used as a BMP-2 delivery system for bone tissue engineering. J Biomed Mater Res A 2010; 92: 1105-1114.
[11] von Doernberg MC, von Rechenberg B, Bohner M, Grunenfelder S, van Lenthe GH, Muller R, Gasser B, Mathys R, Baroud G and Auer J. In vivo behavior of calcium phosphate scaffolds with four different pore sizes. Biomaterials 2006; 27: 5186-5198.
[12] Kondo N, Ogose A, Tokunaga K, Umezu H, Arai K, Kudo N, Hoshino M, Inoue H, Irie H, Kuroda K, Mera H and Endo N. Osteoinduction with highly purified beta-tricalcium phosphate in dog dorsal muscles and the proliferation of osteoclasts before heterotopic bone formation. Biomaterials 2006; 27: 4419-4427.
[13] Yuan H, Van Den Doel M, Li S, Van Blitterswijk CA, De Groot K and De Bruijn JD. A comparison of the osteoinductive potential of two calcium phosphate ceramics implanted intramuscularly in goats. J Mater Sci Mater Med 2002; 13: 1271-1275.
[14] Seebach C, Henrich D, Schaible A, Relja B, Jugold M, Bonig H and Marzi I. Cell-based therapy by implanted human bone marrow-derived mononuclear cells improved bone healing of large bone defects in rats. Tissue Eng Part A 2015; 21: 1565-1578.
[15] Nagahara T, Yoshimatsu S, Shiba H, Kawaguchi H, Takeda K, Iwata T, Mizuno N, Fujita T and Kurihara H. Introduction of a mixture of beta-tricalcium phosphate into a complex of bone marrow mesenchymal stem cells and type I collagen can augment the volume of alveolar bone without impairing cementum regeneration. J Periodontol 2015; 86: 456-464.
[16] Maes C, Kobayashi T, Selig MK, Torrekens S, Roth SI, Mackem S, Carmeliet G and Kronenberg HM. Osteoblast precursors, but not mature osteoblasts, move into developing and fractured bones along with invading blood vessels. Dev Cell 2010; 19: 329-344.
[17] Granero-Molto F, Weis JA, Miga MI, Landis B, Myers TJ, O'Rear L, Longobardi L, Jansen ED, Mortlock DP and Spagnoli A. Regenerative effects of transplanted mesenchymal stem cells in fracture healing. Stem Cells 2009; 27: 1887-1898.
[18] Chen L, Tredget EE, Wu PY and Wu Y. Paracrine factors of mesenchymal stem cells recruit macrophages and endothelial lineage cells and enhance wound healing. PLoS One 2008; 3: e1886.
[19] Yuan J, Cui L, Zhang WJ, Liu W and Cao Y. Repair of canine mandibular bone defects with bone marrow stromal cells and porous beta-tricalcium phosphate. Biomaterials 2007; 28: 1005-1013.
[20] Sukul M, Nguyen TB, Min YK, Lee SY and Lee BT. Effect of Local Sustainable Release of BMP2-VEGF from Nano-Cellulose Loaded in Sponge Biphasic Calcium Phosphate on Bone Regeneration. Tissue Eng Part A 2015; 21: 1822-1836.
[21] Kumar S, Wan C, Ramaswamy G, Clemens TL and Ponnazhagan S. Mesenchymal stem cells expressing osteogenic and angiogenic factors synergistically enhance bone formation in a mouse model of segmental bone defect. Mol Ther 2010; 18: 1026-1034.
[22] Kempen DH, Lu L, Heijink A, Hefferan TE, Creemers LB, Maran A, Yaszemski MJ and Dhert WJ. Effect of local sequential VEGF and BMP-2 delivery on ectopic and orthotopic bone regeneration. Biomaterials 2009; 30: 2816-2825.
[23] Curtin CM, Tierney EG, McSorley K, Cryan SA, Duffy GP and O'Brien FJ. Combinatorial gene

therapy accelerates bone regeneration: non-viral dual delivery of VEGF and BMP2 in a collagen-nanohydroxyapatite scaffold. Adv Healthc Mater 2015; 4: 223-227.
[24] Shah RK, Moncayo VM, Smitson RD, Pierre-Jerome C and Terk MR. Recombinant human bone morphogenetic protein 2-induced heterotopic ossification of the retroperitoneum, psoas muscle, pelvis and abdominal wall following lumbar spinal fusion. Skeletal Radiol 2010; 39: 501-504.
[25] Desai KGH and Schwendeman SP. Active self-healing encapsulation of vaccine antigens in PLGA microspheres. J Control Release 2013; 165: 62-74.
[26] Shah RB and Schwendeman SP. A biomimetic approach to active self-microencapsulation of proteins in PLGA. J Control Release 2014; 196: 60-70.
[27] Sun Z, Tee BC, Kennedy KS, Kennedy PM, Kim DG, Mallery SR and Fields HW. Scaffold-based delivery of autologous mesenchymal stem cells for mandibular distraction osteogenesis: preliminary studies in a porcine model. PLoS One 2013; 8: e74672.
[28] Sun Z, Kennedy KS, Tee BC, Damron JB and Allen MJ. Establishing a critical-size mandibular defect model in growing pigs: characterization of spontaneous healing. J Oral Maxillofac Surg 2014; 72: 1852-1868.
[29] Osugi M, Katagiri W, Yoshimi R, Inukai T, Hibi H and Ueda M. Conditioned media from mesenchymal stem cells enhanced bone regeneration in rat calvarial bone defects. Tissue Eng Part A 2012; 18: 1479-1489.
[30] Geuze RE, Theyse LF, Kempen DH, Hazewinkel HA, Kraak HY, Oner FC, Dhert WJ and Alblas J. A differential effect of bone morphogenetic protein-2 and vascular endothelial growth factor release timing on osteogenesis at ectopic and orthotopic sites in a large-animal model. Tissue Eng Part A 2012; 18: 2052-2062.
[31] Schonmeyr BH, Soares M, Avraham T, Clavin NW, Gewalli F and Mehrara BJ. Vascular endothelial growth factor inhibits bone morphogenetic protein 2 expression in rat mesenchymal stem cells. Tissue Eng Part A 2010; 16: 653-662.
[32] Peng H, Usas A, Olshanski A, Ho AM, Gearhart B, Cooper GM and Huard J. VEGF improves, whereas sFlt1 inhibits, BMP2-induced bone formation and bone healing through modulation of angiogenesis. J Bone Miner Res 2005; 20: 2017-2027.
[33] Li P, Bai Y, Yin G, Pu X, Huang Z, Liao X, Chen X and Yao Y. Synergistic and sequential effects of BMP-2, bFGF and VEGF on osteogenic differentiation of rat osteoblasts. J Bone Miner Metab 2014; 32: 627-635.
[34] Reinhold SE, Desai KG, Zhang L, Olsen KF, Schwendeman SP. Self-Healing Microencapsulation of Biomacromolecules without Organic Solvents. Angew Chem Int Ed Engl 2012; 51: 10800-10803.
[35] Zhu G, Mallery SR and Schwendeman SP. Stabilization of proteins encapsulated in injectable poly (lactide- co-glycolide). Nat Biotechnol 2000; 18: 52-57.
[36] Perez C, Castellanos IJ, Costantino HR, Al-Azzam W and Griebenow K. Recent trends in stabilizing protein structure upon encapsulation and release from bioerodible polymers. J Pharm Pharmacol 2002; 54: 301-313.
[37] Arahira T and Todo M. Effects of proliferation and differentiation of mesenchymal stem cells on compressive mechanical behavior of collagen/beta-TCP composite scaffold. J Mech Behav Biomed Mater 2014; 39: 218-230.
[38] Koepp HE, Schorlemmer S, Kessler S, Brenner RE, Claes L, Gunther KP and Ignatius AA. Biocompatibility and osseointegration of beta-TCP: histomorphological and biomechanical studies in a weight-bearing sheep model. J Biomed Mater Res B Appl Biomater 2004; 70: 209-217.
[39] Lu J, Descamps M, Dejou J, Koubi G, Hardouin P, Lemaitre J and Proust JP. The biodegradation mechanism of calcium phosphate biomaterials in bone. J Biomed Mater Res 2002; 63: 408-412.
[40] Ghanaati S, Barbeck M, Detsch R, Deisinger U, Hilbig U, Rausch V, Sader R, Unger RE, Ziegler G and Kirkpatrick CJ. The chemical composition of synthetic bone substitutes influences tissue reactions in vivo: histological and histomorphometrical analysis of the cellular inflammatory response to hydroxyapatite, beta-tricalcium phosphate and biphasic calcium phosphate ceramics. Biomed Mater 2012; 7: 015005.

Supplementary Data

Materials and methods

Materials

Poly(lactic-co-glycolic acid) (PLGA) 50:50 (i.v. = 0.6 dL/g, M_w = 53.2 kDa, end-group = lauryl ester) was purchased from Durect Corporation (Pelham, AL, USA). PLGA 50:50 (Resomer® RG 502; i.v. = 0.19 dL/g; end-group = alkyl ester) were purchased from Boehringer-Ingelheim GmbH (Ingelheim, Germany). Vascular endothelial growth factor (VEGF) and bone morphogenetic protein 2 (BMP-2) were received from Genentech Inc. (South San Francisco, CA, USA) and Pfizer (Cambridge, MA, USA), respectively. Human VEGF (hVEGF) ELISA development kit (consisted of antigen-affinity purified rabbit anti-hVEGF (capture antibody), biotinylated antigen-affinity purified rabbit anti-hVEGF (detection antibody), hVEGF standard, and avidin-horseradish peroxidase (avidin-HRP) conjugate) and BMP-2 ELISA development kit (consisted of antigen-affinity purified rabbit anti-hBMP-2 (capture antibody), biotinylated antigen-affinity purified rabbit anti-hBMP-2 (detection antibody), hBMP-2 standard, and avidin-horseradish peroxidase (avidin-HRP) conjugate) were purchased from PeproTech (Rocky Hill, NJ, USA). ABTS (2,2'-azino-di-(3-ethylbenzthiazoline-6-sulfonate) liquid substrate solution, magnesium carbonate ($MgCO_3$) and bovine serum albumin (BSA) were purchased from Sigma (St. Louis, MO, USA).

Preparation of VEGF or BMP-2 encapsulated PLGA microspheres

Encapsulation of VEGF or BMP-2 in PLGA microspheres was performed by a water-in-oil-in-water (w/o/w) emulsion-solvent evaporation method. Briefly, appropriate volume (75-200 µL) of inner water phase (VEGF: 5 mg/mL VEGF + 94 mg/mL trehalose in 5 mM succinate buffer (pH 5.0) or 2.44 mg/mL VEGF + 72.5 mg/mL BSA in 5 mM succinate buffer (pH 5.0); BMP-2: 4.26 mg/mL BMP-2 + 8.6 mg/mL BSA in buffer (2.5% w/v glycine, 5 mM glutamic acid, 0.5% w/v sucrose, 5 mM NaCl, and 0.01% Tween 80, pH 4.5)) was added to 1 mL of 200 or 250 or 500 mg/mL PLGA with $MgCO_3$ (3 or 6 %w/w) in methylene chloride. The mixture was homogenized at 10-15 000 rpm with a Tempest IQ^2 homogenizer (The VirTis Company, Gardiner, NY, USA) equipped with a 10 mm shaft in an ice/water bath for 1 min to prepare the first emulsion. Two milliliters of 5% (w/v) PVA solution was immediately added to the primary w/o emulsion (PVA at 5% w/v concentration was used as an emulsifier to stabilize w/o/w emulsion), and the mixture was vortexed (Genie 2, Fisher Scientific Industries, Inc., Bohemia, NY, USA) for 60-120 s to produce the w/o/w double emulsion. The parameters studied for the formation of w/o/w double emulsion is given in Supplementary Table 1. The resultant emulsion was poured into 100 mL of 0.5% (w/v) PVA solution under rapid stirring and hardened at room temperature for 3 h (PVA at 0.5% w/v concentration was used as an emulsifier to prevent agglomeration of particles). Hardened microspheres were collected by sieve (20-63 and 63-125 µm), washed repeatedly with double-distilled (dd) H_2O, and freeze-dried.

Loading assay of proteins (VEGF, BMP-2 and BSA)

About 5 mg of PLGA microspheres loaded with VEGF, VEGF + BSA or BMP-2 + BSA were dissolved in 1.5 mL acetone and vortexed for 1 minute. The mixture was centrifuged at 10 000 rpm for 10 min and the supernatant was removed. The residual content was washed twice with acetone through centrifugation/supernatant removal, followed by drying the residue at room temperature for 2 h. To the dried residue, 1 mL of PBS + 0.02% Tween 80 (pH 7.4) (to determine soluble protein (VEGF or VEGF + BSA or BMP-2 + BSA content) or PBS + 0.02% Tween 80 + 1% BSA (pH 7.4) (to determine active VEGF or BMP-2 content) was added and incubated at 37°C for 24 h. After 24 h, the samples were centrifuged at 8,000 rpm for 10 min and the supernatant was analyzed respectively by modified Bradford assay and ELISA to determine the soluble and active protein fractions. To the remaining residue of total protein assay samples, reducing solution (10 mM dl-dithiothreitol + 6 M urea + 1 mM EDTA) was added and incubated at 37°C for 2 h to dissolve any aggregate and centrifuged. The content of aggregates in supernatant was analyzed by a modified Bradford assay.

Coomassie (modified bradford) protein assay

A modified Bradford assay was used to determine soluble and insoluble protein concentrations. Briefly, appropriate volume of standard or sample was mixed with Coomassie Plus® reagent (Thermo Fisher Scientific, Rockford, IL, USA) in a 96-well plate (Nalge Nunc International, Rochester, NY, USA). Then, the absorbance was read at 595 nm within 30 min using a Dynex II MRX microplate reader (Dynex Technology Inc., Chantilly, VA, USA).

Enzyme-Linked immunosorbent assay (ELISA)

The ELISA was performed at room temperature according to the manufacturer's instructions. Briefly, 100 µL of 0.5 µg/mL of capture antibody (antigen-affinity purified rabbit anti-hVEGF (VEGF) or anti-hBMP-2 (BMP-2)) in PBS (pH 7.2) was added to 96-well microtitration plates (Nalge Nunc International, Rochester, NY, USA) and incubated overnight. The plates were washed 4 times between all steps with PBS containing 0.05% Tween® 20. Three hundred microliters of block buffer (PBS containing 1% BSA) was added to each well, incubated for 1 h, and then washed. The diluent used for preparing VEGF, BMP-2 and antibodies samples (except capture antibody above) was PBS containing 0.1% BSA and 0.05% Tween® 20. One hundred microliters of standard VEGF or BMP-2 with known concentration (0.008-100 ng/mL VEGF or 0.1-1000 ng/mL BMP-2) and test samples were added to each well in duplicate, incubated for 2 h and then washed. One hundred microliters of 0.25 (VEGF) or 1 (BMP-2) µg/mL detection antibody (biotinylated antigen-affinity purified rabbit anti-hVEGF or anti-hBMP-2) was added to each well and incubated for 2 h and washed. One hundred microliters of diluted (1:2000 dilution) avidin-HRP conjugate was added to each well and incubated for 2 h. After washing, 100 µL of ABTS liquid substrate solution was to each well and incubated for 30 minutes. The absorbance was read at 405 nm on a Dynex II MRX microplate reader (Dynex Technology Inc., Chantilly, VA, USA) equipped with Revelation 3.2 Software. Log/Logit curve fitting model was used to plot the standard curve and calculate unknown concentration of VEGF or BMP-2 in test samples.

Scanning electron microscopy (SEM)

Surface morphology of active PLGA microspheres was examined by taking SEM images using a Hitachi S3200N scanning electron microscope (Hitachi, Tokyo, Japan). Briefly, microspheres were fixed previously on a brass stub using double-sided adhesive tape and then were made electrically conductive by coating, in a vacuum, with a thin layer of gold (3-5 nm) for 100 s at 40 W. The surface view images of microspheres were taken at an excitation voltage of 8-10 kV.

Supplementary Table 1. The manufacturing conditions and formulation composition for VEGF/PLGA and BMP-2/PLGA microspheres

Formulation conditions and compositions	VEGF formulations						BMP-2 formulations		
	Preparation method (w/o/w or s/o/w) and formulation code (F1-F9)								
	w/o/w				s/o/w		w/o/w		
	F1	F2	F3	F4	F5	F6	F7	F8	F9
PLGA concentration (mg/mL)	200[a]	250[a]	250[a]	500[b]	500[b]	500[b]	500[b]	500[c]	500[b]
Inner water phase volume (mL/1 mL oil phase)	0.15	0.075	0.15	0.15	0.2	-	0.2	0.2	0.2
First homogenization speed (rpm)	15,000	12,000	12,000	10,000	10,000	10,000	10,000	10,000	10,000
First homogenization duration (min)	1	1	1	1	1	1	1	1	1
Second vortexing time (seconds)	60	60	60	60	60	120	60	60	60
Trehalose loading (wt%)	1	-	-	-	-	-	-	-	-
VEGF or BMP-2 loading (wt%)	0.1	0.07	0.14	0.07	0.092	0.09	0.16	0.16	0.16
BSA loading (wt%)	2.9	2.0	4.0	2.07	2.73	2.89	0.32	0.32	0.32
$MgCO_3$ loading (wt%)	3.0	3.0	3.0	3.0	3.0	3.0	3.0	3.0	6.0

[a]PLGA 50:50 (i.v.= 0.6 dL/g, M_w = 53.2 kDa, end-group = lauryl ester). [b]PLGA 50:50 (Resomer® RG 502) (i.v.= 0.19 dL/g, end-group = alkyl ester). [c]PLGA 50:50 (Resomer® RG 502) + PLGA-PEG (mass ratio = 75/25).

Supplementary Table 2. Evaluation of microencapsulation and stability of VEGF and total protein (VEGF + BSA) in PLGA microspheres prepared by water-in-oil-in-water (F1-F4) and solid-in-oil-water (F5) methods

Form.	Particles Size (μm)	Theoretical Loading (wt%)		Actual Loading (wt%)*				Encapsulation Efficiency (%)*	
		VEGF	Total Protein (VEGF + BSA)	VEGF	Soluble Protein (VEGF + BSA)	Insoluble Protein (VEGF + BSA)	Total Protein (VEGF + BSA)	VEGF	Total Protein (VEGF + BSA)
F1	20-63	0.10	3.0	0.017 ± 0.001	0.88 ± 0.03	0.20 ± 0.01	1.1 ± 0.04	17.0 ± 0.7	36.8 ± 1.3
F2	20-63	0.07	2.07	0.030 ± 0.002	1.66 ± 0.06	0.33 ± 0.04	2.0 ± 0.10	43.3 ± 2.8	95.8 ± 3.8
	63-125	0.07	2.07	0.024 ± 0.002	1.28 ± 0.04	0.23 ± 0.03	1.5 ± 0.05	34.9 ± 2.2	72.8 ± 2.6
F3	20-63	0.14	4.14	0.048 ± 0.004	2.40 ± 0.12	0.39 ± 0.07	2.8 ± 0.18	34.6 ± 2.7	67.3 ± 4.5
	63-125	0.14	4.14	0.032 ± 0.003	1.79 ± 0.04	0.26 ± 0.01	2.0 ± 0.04	22.8 ± 2.1	48.9 ± 1.0
F4	20-63	0.07	2.07	0.030 ± 0.001	1.10 ± 0.07	0.33 ± 0.04	1.4 ± 0.11	27.8 ± 6.0	68.4 ± 5.1
F5	20-63	0.092	2.82	0.034 ± 0.005	1.73 ± 0.10	0.49 ± 0.05	2.2 ± 0.12	37.1 ± 5.0	78.8 ± 4.1
F6	20-63	0.09	2.89	0.024 ± 0.001	0.82 ± 0.20	0.29 ± 0.07	1.1 ± 0.27	20.2 ± 3.0	37.8 ± 9.2

*Mean ± SEM, n = 3.

Supplementary Table 3. Evaluation of microencapsulation and stability of BMP-2 and total protein (BMP-2 + BSA) in PLGA microspheres prepared by water-in-oil-in-water emulsion-solvent evaporation

Form.	Theoretical Loading (wt%)		Actual Loading (wt%)*				Encapsulation Efficiency (%)*	
	BMP-2	Total Protein (BMP-2 + BSA)	BMP-2	Soluble Protein (BMP-2 + BSA)	Insoluble Protein (BMP-2 + BSA)	Total Protein (BMP-2 + BSA)	BMP-2	Total Protein (BMP-2 + BSA)
F7	0.16	0.48	0.060 ± 0.002	0.27 ± 0.01	0.07 ± 0.01	0.35 ± 0.01	37.7 ± 1.0	72.2 ± 3.1
F8	0.16	0.48	0.020 ± 0.001	0.14 ± 0.01	0.06 ± 0.01	0.20 ± 0.02	12.4 ± 0.6	41.5 ± 4.3
F9	0.16	0.48	0.057 ± 0.003	0.30 ± 0.02	0.07 ± 0.02	0.37 ± 0.02	35.6 ± 1.3	77.1 ± 4.6

*Mean ± SEM, n = 3. F7: PLGA (Resomer RG 502)/0.16 wt% BMP-2/0.32 wt% BSA/3 wt% $MgCO_3$ microspheres. F8: PLGA (Resomer RG 502) + PLGA-PEG (75/25)/0.16 wt% BMP-2/0.32 wt% BSA/3 wt% $MgCO_3$ microspheres. F9: PLGA (Resomer RG 502)/0.16 wt% BMP-2/0.32 wt% BSA/6 wt% $MgCO_3$ microspheres.

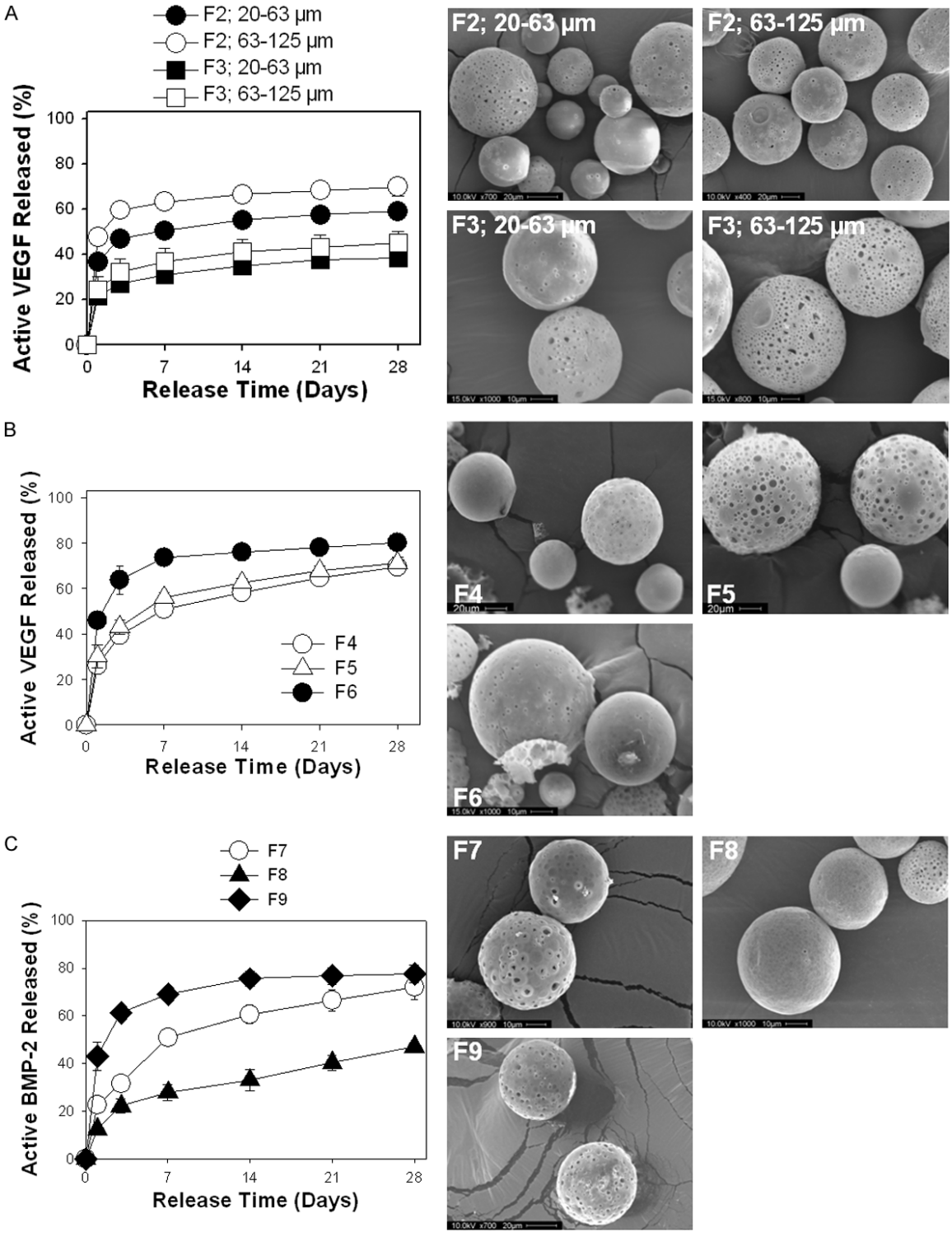

Supplementary Figure 1. A. The effect of manufacturing parameters (inner water phase-to-1 mL oil phase ratio and microspheres size) (F2 and F3 in Supplementary Table 1) on *in vitro* release of VEGF from PLGA microspheres. B. The effect of encapsulation method w/o/w (F4 and F5 in Supplementary Table 1) or s/o/w (F6 in Supplementary Table 1) on *in vitro* release of VEGF from PLGA microspheres. C. S3. The effect of $MgCO_3$ loading and blending (75/25 mass ratio) of low Mw PLGA (0.19 dL/g) with medium Mw PLGA-PEG block copolymer (F7-F9, Supplementary Table 1) on *in vitro* release of BMP-2 from PLGA microspheres.